

## Study on Damping Characteristics of Hydropneumatic Suspension Unit of Tracked Vehicle

**Jin-Rae Cho\*, Hong-Woo Lee, Wan-Suk Yoo**

*School of Mechanical Engineering, Pusan National University,  
Jangjeon-Dong, Kumjung-Ku, Pusan 609-735, Korea*

**Jin-Kyu Lee**

*Tong Myung Heavy Industries Co., Changwon, Kyungnam 641-050, Korea*

Hydropneumatic suspension unit is an important part of tracked vehicles to absorb external impact load exerted from the non-paved road and the cannon discharge. Its absorption performance is strongly influenced by both damping and spring forces of the unit. In this paper, we numerically analyze the damping characteristics of the in-arm-type hydropneumatic suspension unit (ISU) by considering four distinct dynamic modes of the ISU damper : jounce-loading, jounce-unloading, rebound-loading and rebound-unloading. The flow rate coefficients determining the oil flow rate through the damper orifice are decided with the help of independent experiments. The wheel reaction force, the flow rate at cracking and the damping energy are parametrically investigated with respect to the orifice diameter and the wheel motion frequency.

**Key Words :** ISU, Damping Characteristics, Damper Dynamic Mode, Damper Orifice, Flow Rate Coefficients, Flow Rate at Cracking, Damping Energy

### 1. Introduction

Differing from general vehicles running on well-paved road, heavy-weighted tracked vehicle travels on non-paved rugged road with relatively high speed. Furthermore, it is subjected to a very big rebounding impact at the time of the cannon discharge. As a result, oscillatory impact loads exerted from such a non-paved road or/and the cannon discharge may, but frequently, cause the vehicle damage, the running performance degradation and the loss of maneuverability. Referring to Figs. 1 and 2 representing the schematic views of general armed tracked vehicle and the suspension unit, each wheel is assembled into the tracked

vehicle through the suspension unit in order to absorb the external impact load.

Here, the absorption process of a hydropneumatic suspension unit is accomplished by a combination of spring and damping forces (Tong Myung Technical Reports 1996, 2000). In general, the absorption performance is mostly characterized by the key component called the damper composed of an orifice and disc springs installed within the suspension unit. Thus, an appropriate hydrodynamic modeling of the damper is essential for the accurate prediction of the dynamic damping performance (Tong Myung Technical Reports 2002).

Hydropneumatic suspension unit is classified into two types, ISU (in-arm-type hydropneumatic suspension unit) and HSU (hydro-pneumatic suspension unit) according to the layout of the arm. In the former case arm and main housing are unified into a body (refer to Fig. 2), but the arm is positioned outside the main housing in the latter case. Therefore, both show remarkable

---

\* Corresponding Author,

E-mail : jrcho@hyowon.pusan.ac.kr

TEL : +82-51-510-2467; FAX : +82-51-514-7640

School of Mechanical Engineering, Pusan National University, Jangjeon-Dong, Kumjung-Ku, Pusan 609-735, Korea. (Manuscript Received August 29, 2003; Revised November 14, 2003)

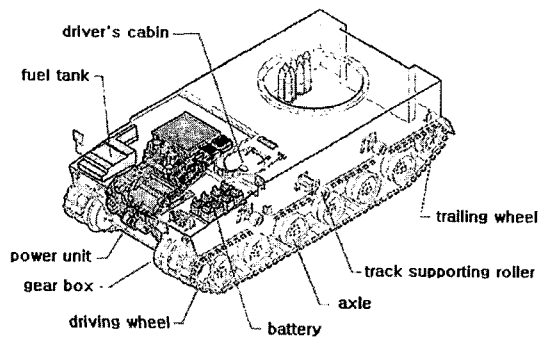


Fig. 1 Major components of armed tracked vehicle

differences in the kinematic motion as well as the structural composition. Regarding the dynamic characteristics and the design of HSU the reader may refer to the Tong Myung technical report (2002 in Korean).

The main purpose of this paper is to investigate the damping characteristics of ISU. The dynamic motion of ISU is split into four; jounce-loading, jounce-unloading, rebound-loading and rebound-unloading, so that four distinct dynamic modes should be considered for the damper. Here, jounce and rebound are distinguished whether the wheel moves upward or downward from its stationary position (SP), meanwhile loading and unloading are judged by compression or release of disc springs in the damper, which will be clear in following sections. In order to accurately calculate the oil flow rate through the damper orifice, we determine the flow coefficients using experimental results. After constructing the mathematical damping models, we perform the parametric experiments to examine the effects of the orifice diameter and the wheel motion frequency on the ISU damping performance.

## 2. Structure and Kinematics of ISU

### 2.1 Structure and operating mechanism of ISU

Referring to Fig. 2(a), an ISU is attached to the tracked vehicle via a mounting plate and a vehicle wheel is assembled into ISU. But, the assembly of ISU and wheel is permitted to rotate about the fixed arm axis, so that the vehicle wheel moves upward (jounce) or downward (rebound)

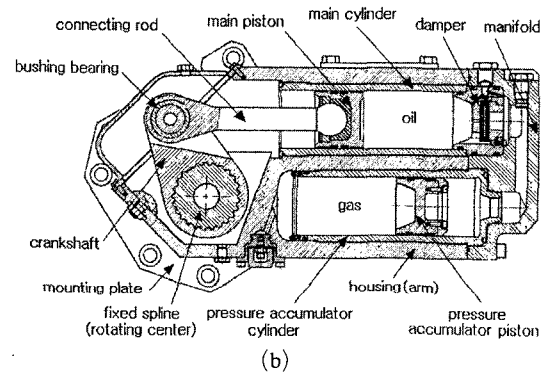
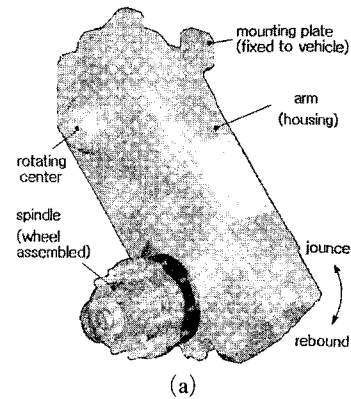


Fig. 2 ISU : (a) assembled configuration ; (b) schematic view of its components

from the stationary position. Then, referring to Fig. 2(b), the main piston moves relatively in the direction compressing oil contained in the main cylinder when ISU is in the jounce mode, and vice versa. The main cylinder and the PA (pressure accumulator) cylinder are open-channeled along the manifold such that oil can flow from the right side of the main piston up to the left side of the PA (pressure accumulator) piston. Differing from the damper fixed at the right end of the main cylinder, the PA piston moves horizontally according to oil and gas pressures. Of course, the left end of the PA cylinder is closed.

When ISU is in the jounce mode, the relative rotation of ISU housing about the rotating center makes the main piston compress oil. Then, oil is forced to pass through the damper and compress the PA piston until the force balance between gas and oil is reached. On the other hand, in the rebound mode ISU rotates down by the expansion of gas in the PA cylinder. In this manner,

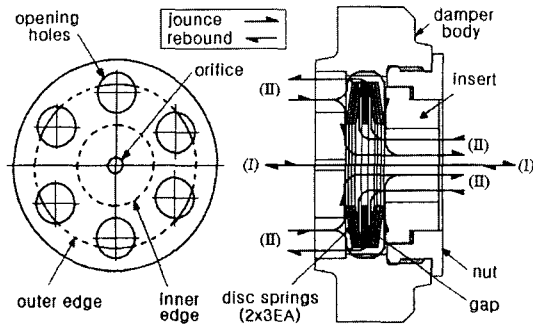


Fig. 3 Damper assembly

the external oscillatory impact can be absorbed. Referring to Fig. 3, the damper is composed of an orifice, opening holes, pre-compressed disc springs, a disc-type gap, a nut and an insert. Regardless of the oil pressure magnitude, the main flow path (I) from the orifice to the damper exit through inner holes of disc springs and gap is opened.

On the other hand, oil can flow along the secondary path (II) only when either disc springs are compressed towards the gap hinged at the spring outer edge or expanded from the gap hinged about the spring inner edge. Initially, an assembly of disc springs is forced to tightly contact with both the orifice core plate and the insert surface. However, sufficiently high oil pressure compresses the disc springs towards the gap in the jounce mode and expands the outer edge of disc springs from the gap, while opening the secondary oil path, so that oil flows along both path (I) and path (II). Here, we define two nomenclatures, cracking and choking. The former indicates the time when disc springs start to compress or expand, while the latter is called when disc springs are completely compressed or expanded. Furthermore, the damper is called in loading status when disc springs move from cracking to choking and in unloading status when those release from choking to cracking.

**2.2 Kinematics of ISU**

The wheel locations at the stationary position (SP), the full jounce (FJ) and the full rebound (FR) are represented in Fig. 4. For the kinematics analysis, we use the local coordinates x-y

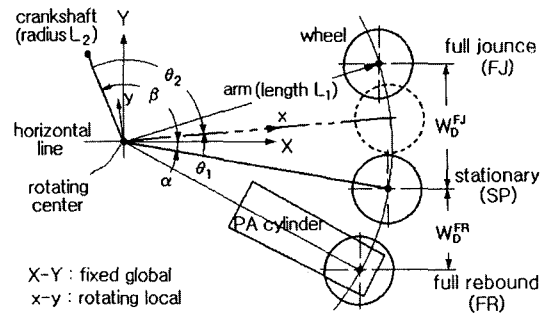


Fig. 4 Coordinate definition and the wheel location

rotating with the ISU arm with respect to the fixed global coordinates X-Y. Here, both coordinate systems are originated at the rotating center. At the stationary position, the arm and the fixed crankshaft are aligned with preset angles  $\alpha$  and  $\beta$ , respectively, with respect to the horizontal line (i.e. the X-axis). For the arm in arbitrary wheel location, we define two angles,  $\theta_1$  from the stationary arm position and  $\theta_2$  from the fixed crankshaft. Since both angles should satisfy the relation:  $\theta_1 + \theta_2 = \alpha + \beta$ , we have  $\dot{\theta}_2 = -\dot{\theta}_1$  and  $\ddot{\theta}_2 = -\ddot{\theta}_1$ .

Figure 5 shows the geometric relationship between ISU components at arbitrary wheel position, where  $D_m$  and  $D_p$  are the diameters of the main and the PA pistons while  $d_m$  and  $d_p$  are their displacements from the stationary position, respectively. Meanwhile, the horizontal distance  $d_1$  of the main piston and the deviation angle  $\theta_3$  are important parameters to be calculated. To derive these parameters, we use the following geometric relation for the position vector  $r_m$ :

$$r_m = d_1 i + H j = r_2 + r_3 \tag{1}$$

where,  $r_2 = L_2(\cos \theta_2 i + \sin \theta_2 j)$  and  $r_3 = L_2(\cos \theta_3 i + \sin \theta_3 j)$ . Then, we can derive following relations given by

$$d_1 = L_2 \cos \theta_2 + [(L_2 \cos \theta_2)^2 - \Lambda]^{1/2} \tag{2}$$

with  $\Lambda = L_2^2 + H^2 - L_3^2 - 2L_2 \sin \theta_2$ , and

$$\theta_3 = \tan^{-1} \left[ \frac{H - L_2 \sin \theta_2}{d_1 - L_2 \cos \theta_2} \right] \tag{3}$$

Using Eqs. (1) and (2), we can also derive the main piston velocity  $v_m (= \dot{d}_1 = -\dot{d}_m)$  given by

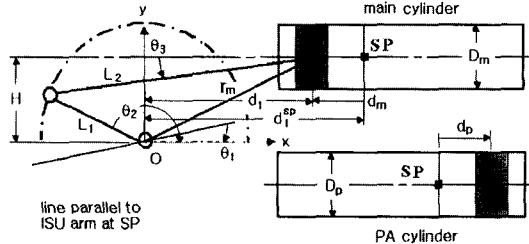


Fig. 5 Angles and position vectors at arbitrary wheel position

$$v_m = L_2 (\tan \theta_3 \cos \theta_2 - \sin \theta_2) \dot{\theta}_2 \quad (4)$$

Furthermore,

$$d_p = D_g d_m / D_m, \quad v_p = D_g v_m / D_m \quad (5)$$

We note here that both piston velocities are positive when both pistons are in the jounce mode.

Fig. 6 depicts forces acting on ISU, where the oil pressure  $p$  is the sum of the oil pressure drop  $p_d$  through the damper and the gas pressure in the PA cylinder :

$$p = p_d + p_g^i [l_g / (l_g - d_p)]^{1.4} \quad (6)$$

In which,  $l_g$  indicates the PA cylinder length filled with gas which is assumed to be an ideal gas, at the stationary position. The derivation of the oil pressure drop will be given in the next section. When the oil pressure is known, forces acting on the connecting rod and the wheel can be derived. First, the connecting rod force  $F_c$  is calculated through

$$F_c = [F_p \tan^2 \theta_3 + (F_p + F_f)^2]^{1/2} \quad (7)$$

with  $F_p = \pi R_m^2 P$  and  $F_f = \text{sgn}(v_m) \mu |F_p \tan \theta_3|$ . Then, the moment equilibrium about the rotating center gives us the normal force  $F_w$  acting on the wheel given by

$$F_w = F_c L_2 \sin(\theta_2 - \theta_3) / L_1 \cos(\theta_1 - \alpha) \quad (8)$$

Referring to Fig. 4, we assume in the current study the time history of the wheel vertical displacement that brings the ISU mechanism in motion :

$$W_D = \frac{W_D^{FJ} + W_D^{FR}}{2} \sin(2\pi f t - \phi) + \frac{W_D^{FJ} - W_D^{FR}}{2} \quad (9)$$

The frequency and the phase angle in the wheel vertical motion are derived respectively by

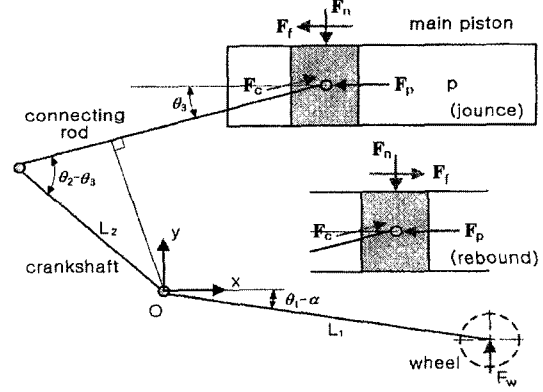


Fig. 6 Forces acting on the main piston and the wheel

$$f = \frac{W_D^{\max}}{\pi (W_D^{FJ} + W_D^{FR})}, \quad \phi = \sin^{-1} \left[ \frac{W_D^{FJ} - W_D^{FR}}{W_D^{FJ} + W_D^{FR}} \right] \quad (10)$$

And, the arm angle  $\theta_1$  is related to the wheel vertical displacement  $W_D$  :

$$\theta_1 = \alpha - \sin^{-1} [(L_1 \sin \alpha - W_D) / L_1] \quad (11)$$

### 2.3 Spring force

Referring to Fig. 7(a), the spring force  $F_s$  acting on a single disc spring is calculated according to (Wahl, 1963)

$$F_s = \frac{4Et^3s}{(1-\nu^2)K_s d_o^2} \left[ \left( \frac{h}{t} - \frac{s}{t} \right) \left( \frac{h}{t} - \frac{s}{2t} \right) + 1 \right] \quad (12)$$

where  $E$  is the Young's modulus and  $\nu$  is the Poisson's ratio of disc spring. On the other hand,  $K_s = [(\zeta - 1)/\zeta]^2 / \pi [(\zeta + 1)/(\zeta - 1) - 2/\ln \zeta]$  in terms of the ratio  $\zeta$  defined by  $\zeta = d_o/d_i$ . Meanwhile, disc springs in the damper shown in Fig. 3 are connected such that each three springs are in parallel connection and two sets composed of three springs are in serial connection. Then, the total spring force  $F_{comb}$  and the displacement  $S_{comb}$  are calculated using

$$F_{comb} = \frac{n_p F_s}{\mu_{comb}}, \quad S_{comb} = n_s s \quad (13)$$

where  $n_p$  and  $n_s$  are spring numbers in parallel and the serial connection number, respectively. And,  $\mu_{comb} = 1 \pm (1 - n_p) \mu$  is the total friction coefficient between springs when  $\mu$  is denoted by the friction coefficient between any two disc springs in parallel connection (+ : loading, - :

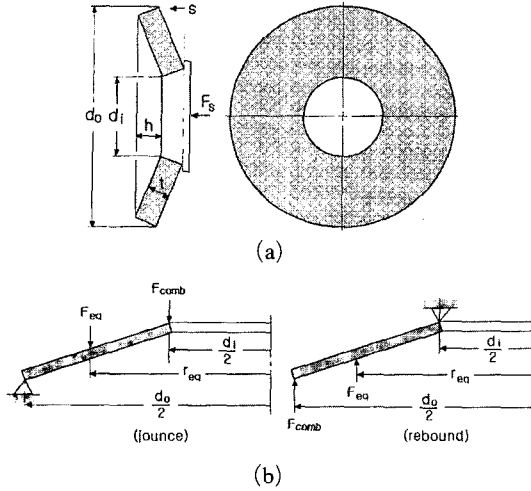


Fig. 7 Disc spring: (a) edge force; (b) equivalent force and its acting position

unloading).

Referring to Fig. 7(a), the equivalent concentration force  $F_{eq}$  of total oil pressure acting on disc springs is  $F_{eq} = \pi p_d (d_o^2 - d_i^2) / 4$  and its acting position  $r_{eq}$  is  $(d_o^3 - d_i^3) / 3(d_o^2 - d_i^2)$ . Then, the total spring force  $F_{comb}$  can be determined using the moment equilibrium such that

$$F_{comb} = \frac{\pi}{4} a (d_o + d_i) p_d \quad (14)$$

where  $a$  is  $(d_o - 2r_{eq})$  in the jounce mode and  $(2r_{eq} - d_i)$  in the rebound mode. As can be inferred from Eqs. (13) and (14), the ISU damper exhibits four distinct damping characteristics according to four damper modes: jounce-loading, jounce-unloading, rebound-loading and rebound-unloading. Meanwhile, the cracking point of the damper varies with the spring pre-load  $F_{pre}$  acting exerted by nut in the damper, so that the damping characteristic can be controlled by adjusting the spring pre-displacement  $s_{pre}$ . In this case, the actual spring displacement  $s_{dm}$  becomes

$$s_{dm} = s_{comb} - s_{pre} \quad (15)$$

### 3. Oil Flow Rate and Pressure Drop Through Damper

In this section, we derive the pressure drop

through the damper in three spring motions, before cracking, from cracking to choking, and after choking. We denote the parameters used for the flow and pressure drop analysis in Fig. 8, where  $p_1$  and  $Q_0$  are the oil pressure and the oil flow rate in the main cylinder. Here,  $Q_0$  is calculated from the main piston velocity  $v_m$  such that (+ : jounce, - : rebound)

$$Q_0 = \pm \pi d_m^2 |v_m| / 4 \quad (16)$$

Assuming incompressible oil flow, pressure drops (Gerhart et al. 1992) through individual damper parts are

$$\Delta p_{12} = p_1 - p_2 = \rho (Q_1 / C_1 A_1)^2 / 2 \quad (17a)$$

$$\Delta p_{32} = p_3 - p_2 = \rho (Q_2 / C_2 A_2)^2 / 2 \quad (17b)$$

$$\Delta p_{43} = p_4 - p_3 = \rho (Q_3 / C_3 A_3)^2 / 2 \quad (17c)$$

$$\Delta p_{14} = p_1 - p_4 = \rho (Q_4 / C_4 A_4)^2 / 2 \quad (17d)$$

where  $C_i$  are the flow rate coefficients to be determined, and  $A_i$  are areas of individual flow holes. Here,  $A_3$  is variable depending on the actual spring displacement  $s_{dm}$ . Then, the pressure drop through the damper  $p_d$  becomes

$$p_d = \Delta p_{12} = \Delta p_{13} + \Delta p_{32} \quad (18)$$

Meanwhile, the continuity condition requires:  $Q_0 = Q_1 + Q_4 = Q_1 + Q_3 = Q_2$ , but  $Q_3 (= Q_4)$  and  $Q_4$  vanish when cracking does not occur, so that the pressure drop before cracking becomes

$$p_d = \frac{\rho}{2} \left[ \left( \frac{1}{C_1 A_1} \right)^2 + \left( \frac{1}{C_2 A_2} \right)^2 \right] Q_0^2 \quad (19)$$

On the other hand, disc springs start to crack when  $F_{comb}$  reaches the spring pre-load  $F_{pre}$ , then the pressure drop at the cracking point is calculated using Eq. (14):

$$p_d^{cra} = \frac{4}{\pi a (d_o + d_i)} F_{pre} \quad (20)$$

And, the flow rate  $Q_0^{cra}$  in the main cylinder can be derived using Eq. (19) such that

$$Q_0^{cra} = \sqrt{P_d^{cra} / \frac{\rho}{2} \left[ \left( \frac{1}{C_1 A_1} \right)^2 + \left( \frac{1}{C_2 A_2} \right)^2 \right]} \quad (21)$$

Oil flow rate gradually increases after cracking and disc springs reach the choking point when

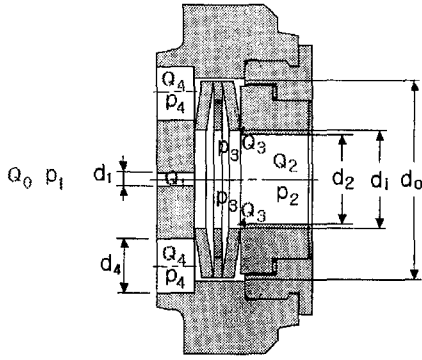


Fig. 8 Parameters for the flow and pressure analysis

$s_{dm}$  becomes  $h$  (refer to Fig. 7(a)). After cracking, it is convenient for calculating  $Q_1$  and  $Q_3$  to introduce the ratio  $\eta$  between  $Q_1$  and  $Q_3$  ( $=Q_4$ ) which is derived using the relation  $\Delta p_{13} = \Delta p_{14} + \Delta p_{43}$ :

$$\frac{1}{\eta} = \frac{Q_1}{Q_3} = C_1 A_1 \left[ \left( \frac{1}{C_3 A_3} \right)^2 + \left( \frac{1}{C_4 A_4} \right)^2 \right]^{1/2} \quad (22)$$

Since  $A_3$  varies with the actual spring displacement, the ratio  $\eta$  is also in function of  $s_{dm}$ . So, we approximate  $\eta$  as a quadratic function of  $s_{dm}$  using three  $\eta$  values at  $s_{dm}=0$ ,  $h/2$  and  $h$ .

Next, we derive the pressure drops at choking and after choking. From Eq. (14), the pressure drop from the opening holes to disc springs becomes

$$\Delta p_{43}^{cho} = \frac{4}{\pi a (d_o + d_i)} F_{comb}^{cho} \quad (23)$$

Using the relation (13), together with  $Q_1 = Q_0 - Q_3$  and  $Q_2 = Q_0$ , we have the pressure drop through the damper at choking:

$$p_d^{cho} = \frac{\rho}{2} \left[ \left( \frac{Q_0^{cho} - Q_3^{cho}}{C_1 A_1} \right)^2 + \left( \frac{Q_0^{cho}}{C_2 A_2} \right)^2 \right] \quad (24)$$

In the same manner, the pressure drop  $p_d$  after choking is also calculated using Eq. (15) by substituting the flow rates at choking with  $Q_0$  and  $Q_3$ . We remind here that  $Q_0$  and  $Q_3$  are calculated using Eqs. (16) and (22), respectively.

#### 4. Numerical Results

According to the theoretical derivation described so far we coded a test Fortran program which is composed of three parts for analyzing

Table 1 Damper parameters for numerical experiments

Parameters	Values
Spring thickness $t$ and $h$	2.35 mm/1.8 mm
Spring diameters $d_o$ , $d_i$	63.0 mm/31.0 mm
Pre-displacement $s_{pre}$	2.35 mm
Friction coefficient $\mu$	0.0012
Connection number $n_p$ , $n_s$	3/2
Spring Young's modulus $E$	204 GPa
Spring Poisson's ratio $\nu$	0.3
Diameters $d_2$ , $d_4$	28.0 mm/17.0 mm
Flow rate coefficients $C_2$ , $C_4$	1.0/1.0
Oil density $\rho$	947.0 kg/m <sup>3</sup>

the ISU kinematics, calculating disc-spring forces and computing oil flow rates and pressure drops. The wheel vertical motion operating ISU is given according to Eqs. (9) and (10), where  $W_D^{FJ}$  and  $W_D^{FR}$  are set respectively by 362.7 mm and 120.2 mm. The wheel motion frequency  $f$ , as well as the orifice diameter  $d_1$  and two flow rate coefficients  $C_1$  and  $C_3$ , is chosen variable; 0.5, 0.7 and 1.0 Hz for the parametric damping analysis. Other simulation parameters are recorded in Table 1.

##### 4.1 Flow rate coefficients

There are four flow rate coefficients to be determined in order for the flow and dynamic damping analyses; two for the main flow path and the other two for the secondary flow path. Referring to Eq. (16), the pressure drop is in reverse proportional to the product  $(CA)^2$  so that the damping characteristic is less insensitive to the flow path of larger section area. Meanwhile, both four coefficients are not independent variables, but dependent such that  $C_1$  and  $C_2$  are in the main path while  $C_3$  and  $C_4$  are in the secondary path, respectively. By virtue of these features, we let  $C_1$  and  $C_3$  are unknown to be determined using experimental results while setting  $C_2$  and  $C_4$  by unity.

Since the secondary path activates after cracking,  $C_1$  and  $C_3$  can be separately determined such that  $C_1$  before cracking and  $C_3$  after cracking. Fig. 9(a) shows the comparison of the pressure drop with the experimental results conducted

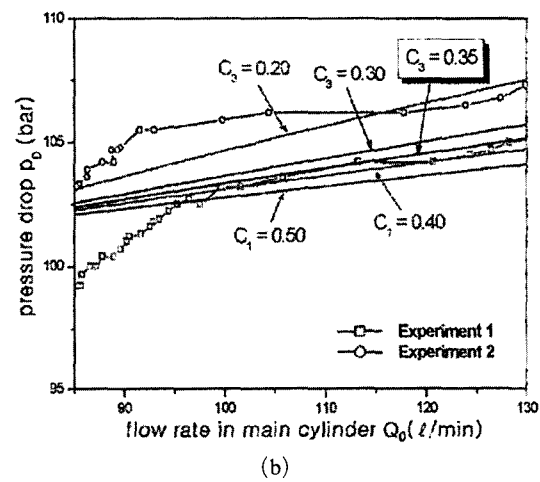
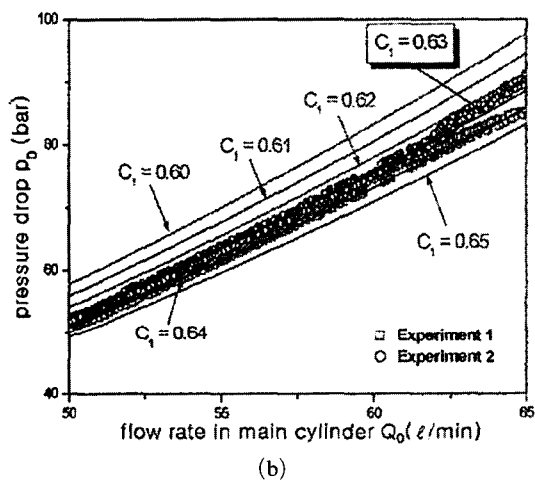
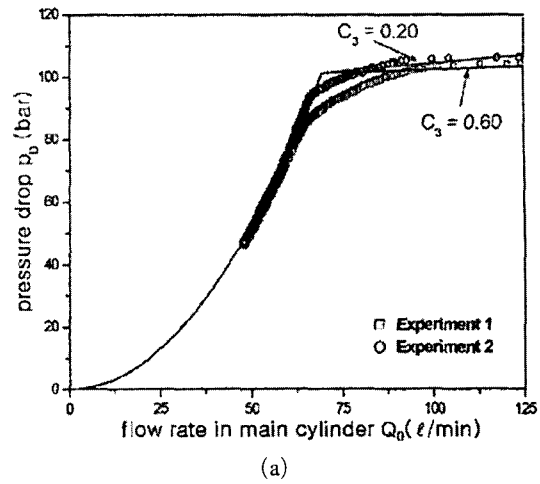
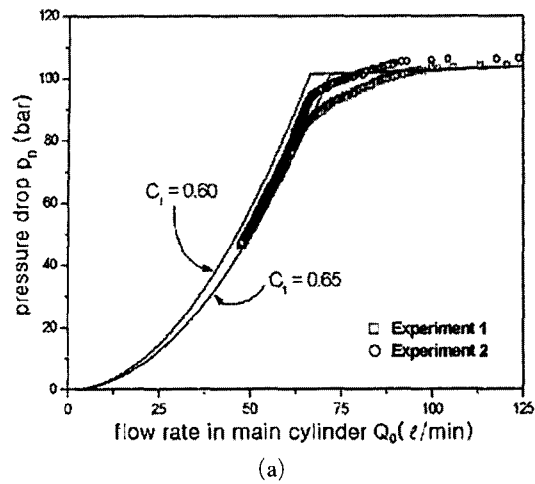


Fig. 9 Flow rate coefficient  $C_1$ : (a) whole period ; (b) before cracking ( $C_3=0.5$ )

Fig. 10 Flow rate coefficient  $C_3$ : (a) whole period ; (b) after cracking ( $C_1=0.63$ )

by Tong Myung. Even though  $C_3$  is tentatively set by 0.5 it does not affect the pressure drop before cracking. From the detailed comparison before cracking in Fig. 9(b), we found that  $C_1$  of 0.63 is appropriate for the current ISU. With  $C_1$  determined we compare the pressure drop after cracking with the experimental results, while varying the flow rate coefficient  $C_3$ . As represented in Fig. 9(b), the choice of  $C_3=0.35$  shows a quite consistent curve with the experimental one. It is worth to note that the value 0.06 and 0.35 are not unique solutions but rather those vary with the preset values of  $C_2$  and  $C_4$ .

We compute the pressure drop  $p_D$  through the damper with the flow rate coefficients determined

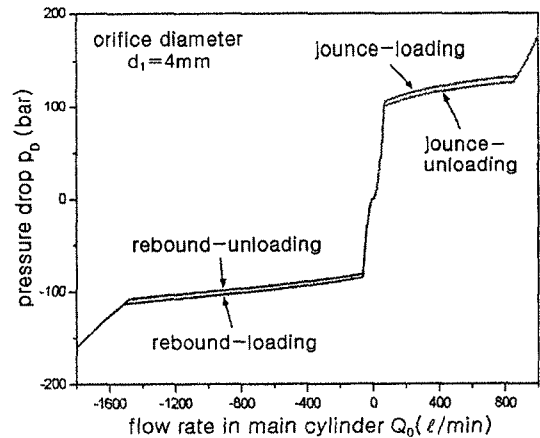


Fig. 11 Pressure drop versus flow rate ( $C_1=0.63$ ,  $C_3=0.35$ )

and present its variation in Fig. 11 to the oil flow rate  $Q_0$  in the main cylinder. Where the right hand side centering about  $Q_0$  is for the jounce mode while the left hand side is for the rebound mode. We first observe the difference in the curve between loading and unloading in the flow rate region starting from cracking to choking, owing to the difference in the hinge point of disc springs. Second, we clearly see the four distinct features of dynamic damping of ISU for four different damper modes, jounce-loading, jounce-unloading, rebound-loading and rebound-unloading.

**4.2 Damping characteristics**

We next perform the parametric analysis for investigating the ISU damping performance to the wheel motion frequency and the orifice diameter. Here, the wheel motion frequency is in proportional relation with the tracked vehicle velocity through rugged road.

Figure 12(a) represents orbits of the wheel reaction force  $F_w$ , during a period of wheel vertical motion, for three different frequencies  $f=0.5, 0.7$  and  $1.0$  Hz, when the orifice diameter  $d_1$  is set by  $4.0$  mm. The reaction force  $F_w$  is calculated using Eq. (6) and the undamped spring force is due only to the gas pressure in the PA cylinder. We see the significant effect of the wheel motion frequency on the ISU damping in both full jounce (FJ) and full rebound (FR) regions such that the damping force increases in proportional to the frequency. Here, the damping force increases as the area inside the closed curve becomes larger. This is because of the difference in cracking occurrence and removal points according to the difference in oil flow rate magnitude caused by wheel motion frequency. Four vertex points in each closed curve in Fig. 12(a) indicate the cracking occurrence or cracking removal points.

Figure 12(b) shows the dependence of the wheel reaction force on the orifice diameter for a fixed wheel motion frequency (i.e. velocity). We first observe that the damping force decreases in proportional to the orifice diameter. Furthermore, there does not occur cracking either in jounce or rebound mode when the orifice diameter reaches  $5$  mm. The flow rate causing cracking increases as

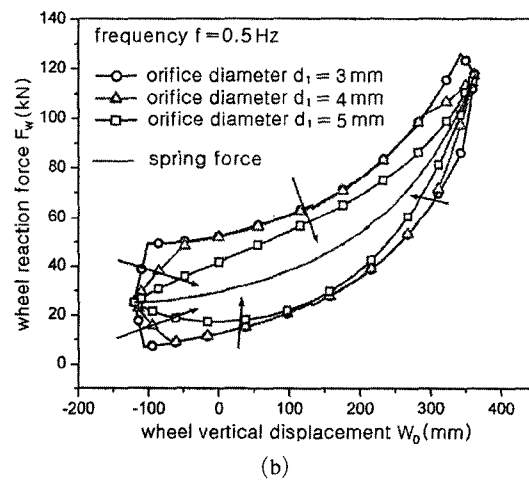
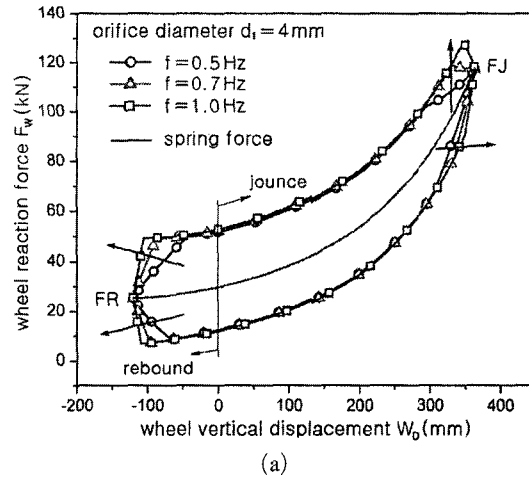


**Fig. 12** Damping characteristics: (a) to the wheel motion frequency; (b) to the orifice diameter

the orifice diameter becomes larger, as represented in Fig. 13(a), so that the wheel vertical velocity should increase for producing the same pressure drop through the damper. In other words, for a given external impact the reacting wheel vertical velocity increases in proportional to the orifice diameter. As a result, one can control the reacting wheel vertical velocity by adjusting the orifice diameter.

Fig. 13(b) represents the parametric variation of the damping energy  $E_D$  absorbed by the damper, during a period of wheel vertical motion, where  $E_D$  is defined by the inside area of the hysteresis curve of  $F_w$  such that



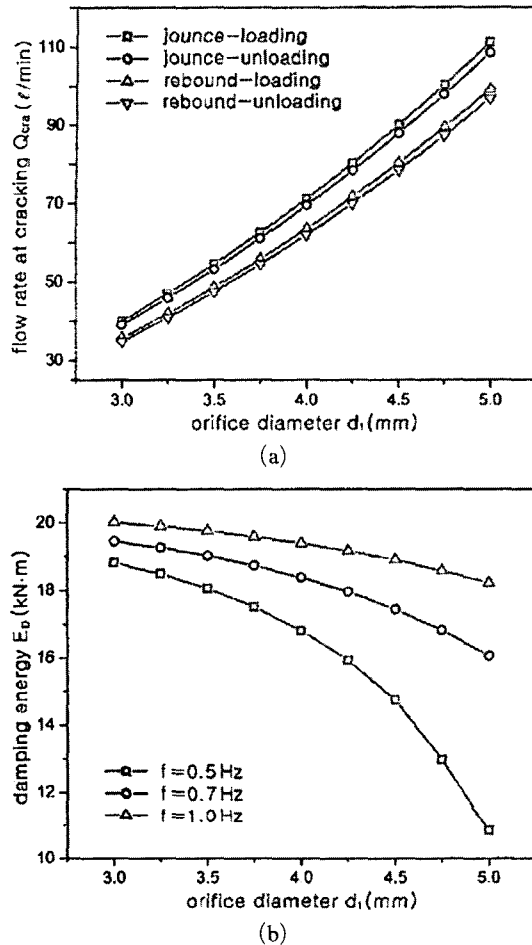


Fig. 13 (a) Flow rate at cracking to the orifice diameter; (b) damping energy during one cycle

$$E_D = \oint F_w dW_D \quad (25)$$

Together with the orifice diameter increase the damping energy monotonically decreases, and the decrease rate becomes considerable as the wheel motion frequency goes lower. From this parametric feature, we can infer the followings. When the orifice diameter is too small, the damper strongly resists to the small external impact before the spring force by gas in the PA cylinder is not fully developed. On the contrary, when the orifice diameter is too large the external impact directly transfers to the PA piston owing to the insufficient impact absorption by the damper, and which makes the wheel vertical displacement be

significantly large. Thus, the cracking pressure should be simultaneously controlled by adjusting the pre-displacement  $S_{pre}$  of disc springs when the orifice diameter is changed, in order to prevent these critical defects.

## 5. Conclusion

The dynamic modeling and numerical investigation for the ISU damping characteristics has been addressed. By classifying the damper dynamic mode into four distinct ones, the oil flow rate and the pressure drop were derived for individual modes. The flow rate coefficients of the damper were determined with the help of independent experiments. From the parametric numerical results, we found that the damping performance and the gas spring force are strongly influenced by the wheel motion frequency and the orifice diameter, while both are in reciprocal relation to two parameters. The larger damping force is produced for either higher frequency or smaller orifice diameter. On the contrary, the gas spring force becomes larger for either lower frequency or wider orifice diameter. Incidentally we found that the damper performance with the suitable wheel vertical displacement can be achieved by adjusting both the orifice diameter and the pre-displacement of disc springs.

## Acknowledgment

The financial supports for this work by Tong Myung Heavy Industries Co., Ltd. and the Korea Science & Engineering Foundation (Grant No.: R01-2001-00383) are gratefully acknowledged. As well, two authors (WSY and HWL) would like to thank the Ministry of Science and Technology of Korea for the financial support by a grant (M1-0203-00-0017-02J0000-00910) under the NRL (National Research Laboratory).

## References

- Black, W. Z. and Hartley, J. G., 1996, *Thermodynamics*, Harper Collins, New York.
- Gerhart, P. M., Gross, R. J. and Hochstein, J. I.,

1992, *Fundamentals of Fluid Mechanics*, Addison-Wesley Publication Company.

Kim, H. O., Lee, H. W., Cho, J. R., Lee, J. K. and Chang, M. S., 2002, "Study on the Kinematic Design of the Hydropneumatic Suspension Unit," *Proc. KSME 2002 Fall Annual Meeting (Pusan Branch)*, pp. 87~92.

Lee, H. W., Cho, J. R., Lee, J. K. and Lee, K. Y., 2003, "Study on Dynamic Design of Reciprocating Hydropneumatic Suspension Unit," *Proc. KSME 2003 Spring Annual Meeting (Pusan Branch)*, pp. 83~88.

Lee, H. W., Kim, H. O., Cho, J. R., Lee, J. K. and Chang, M. S., 2002, "Characteristic Analysis of Spring and Damping of the Hydropneumatic Suspension Unit," *Proc. KSME 2002 Fall Annual Meeting (Pusan Branch)*, pp. 93~98.

Press, W. H., Teukolsky, S. A., Vetterling, W. T. and Flannery, B. P., 1992, *Numerical Recipes in Fortran: The Art of Scientific Computing*, Cambridge University Press.

Tong Myung Heavy Industries Co., Ltd., R&D Center, 1996, *Technical Report: Analysis of Dynamic Behavior and Heat Transfer of HSU*.

Tong Myung Heavy Industries Co., Ltd., R&D Center, 2000, *Technical Report: The Design of ERSU*.

Tong Myung Heavy Industries Co., Ltd., R&D Center, 2002, *Technical Report: The Design and Computational Analysis of HSU Back-Up Model of NIFV ISU*.

Wahl, A. M., 1963, *Mechanical Springs*, McGraw-Hill.